Characterization of apicomplexan amino acid transporters (ApiATs) in the malaria parasite *Plasmodium falciparum*

Jan Stephan Wichers[1,2,3], Carolina van Gelder[1,2,3†*], Gwendolin Fuchs[1,2,3†§], Julia Mareike Ruge[1,2,3], Emma Pietsch[1,2,3], Josie L. Ferreira[1,4], Soraya Safavi[1,2,3], Heidrun von Thien[1,2,3], Paul-Christian Burda[1,2,3], Paolo Mesén-Ramirez[2], Tobias Spielmann[2], Jan Strauss[1,2,3,5], Tim-Wolf Gilberger[1,2,3,#], Anna Bachmann[1,2,3,6,#]

[1] Centre for Structural Systems Biology, 22607 Hamburg, Germany
[2] Bernhard Nocht Institute for Tropical Medicine, 20359 Hamburg, Germany
[3] Biology Department, University of Hamburg, 22609 Hamburg, Germany
[4] Heinrich-Pette-Institute, Leibniz Institute for Experimental Virology, 20251 Hamburg, Germany
[5] GEOMAR Helmholtz Centre for Ocean Research Kiel, 24105 Kiel, Germany
[6] German Center for Infection Research (DZIF), partner site Hamburg-Borstel-Lübeck-Riems, Germany
† contributed equally
* Present address: University of Duisburg-Essen, 45141 Essen, Germany
§ Present address: Karolinska Institutet, 171 77 Stockholm, Sweden
# Corresponding author: gilberger@bnitm.de; bachmann@bnitm.de

ORCID:

Jan Stephan Wichers:	0000-0002-0599-1742
Carolina van Gelder:	0000-0002-8109-3098
Gwendolin Fuchs:	0000-0001-9294-6984
Julia Mareike Ruge:	0000-0002-6295-0293
Emma Pietsch:	0000-0003-4744-1666
Josie L. Ferreira:	0000-0002-4411-6131
Soraya Safavi:	0000-0001-9989-0952
Paul-Christian Burda:	0000-0003-0461-4352
Paolo Mesén-Ramírez:	0000-0001-7842-5867
Tobias Spielmann:	0000-0002-3968-4601
Jan Strauss:	0000-0002-6208-791X
Tim-Wolf Gilberger:	0000-0002-7965-8272
Anna Bachmann:	0000-0001-8397-7308

ABSTRACT

During the symptomatic human blood phase, malaria parasites replicate within red blood cells. Parasite proliferation relies on the uptake of nutrients, such as amino acids, from the host cell and the blood plasma, requiring transport across multiple membranes. Amino acids are delivered to the parasite through the parasite surrounding vacuolar compartment by specialized nutrient-permeable channels of the erythrocyte membrane and the parasitophorous vacuole membrane (PVM). However, further transport of amino acid across the parasite plasma membrane (PPM) is currently not well characterized. In this study, we focused on a family of Apicomplexan amino acid transporters (ApiATs) that comprises five members in *Plasmodium falciparum*. First, we localized four of the *Pf*ApiATs at the PPM using endogenous GFP-tagging. Next, we applied reverse genetic approaches to probe into their essentiality during asexual replication and gametocytogenesis. Upon inducible knockdown and targeted gene disruption a reduced asexual parasite proliferation was detected for *Pf*ApiAT2 and *Pf*ApiAT4. Functional inactivation of individual *Pf*ApiATs targeted in this study had no effect on gametocyte development. Our data suggest that individual *Pf*ApiATs are partially redundant during asexual *in vitro* proliferation and fully redundant during gametocytogenesis of *P. falciparum* parasites.

IMPORTANCE

Malaria parasites live and multiply inside cells. To facilitate their extremely fast intracellular proliferation they hijack and transform their host cells. This also requires the active uptake of nutrients, such as amino acids, from the host cell and the surrounding environment through various membranes that are the consequence of the parasite's intracellular lifestyle. In this manuscript we focus on a family of putative amino acid transporters termed ApiAT. We show expression and localization of four transporters in the parasite plasma membrane of *Plasmodium falciparum*-infected erythrocytes that represent one interface of the pathogen to its host cell. We probed into the impact of functional inactivation of individual transporters on parasite growth in asexual and sexual blood stages of *P. falciparum* and reveal that only two of them show a modest but significant reduction in parasite proliferation but no impact on gametocytogenesis pointing towards redundancy within this transporter family.

INTRODUCTION

Malaria parasites replicate within human erythrocytes during the asexual blood phase, which is responsible for the symptoms of the disease. Although *Plasmodium falciparum* is able to synthesize some amino acids *de novo*[1–6] during the intraerythrocytic development, the parasite rely heavily on amino acid acquisition from its host. Amino acids are derived either from the digestion of hemoglobin endocytosed from the infected erythrocyte[1,7] or from the uptake of free amino acids from the blood plasma[1]. Both processes are important for efficient parasite growth[8]**.** The parasite is able to import all 20 naturally occurring α-amino acids from the external medium and uses them for its own protein synthesis[9–12]. Especially, the import of isoleucine[13–15] – and for some *P. falciparum* strains also methionine[13] – is crucial for the survival of the parasite as adult human hemoglobin lacks isoleucine. Accordingly, an increase in the permeability to a range of amino acids has been reported for erythrocytes upon *Plasmodium* infection[10,11,16,17]. This is mainly mediated via the New Permeability Pathways (NPPs) established by the parasite within the membrane of the infected erythrocyte[16,17]. While the subsequent transport across the parasitophorous vacuole membrane (PVM) is linked to nutrient-permeable channel activity[18–21] the molecular machinery responsible for the further transport across the parasite plasma membrane (PPM) is not well defined. Neutral amino acids like isoleucine and methionine traverse the PPM more rapidly than anionic and cationic amino acids, which may be coupled to the transport of other substrates like H^+ or Na^+ [16,22]. However, neither the membrane transporters nor the exact mechanism(s) by which amino acids cross the PPM have been characterized so far[8,22].

The *P. falciparum* transportome is predicted to be encoded by 144 genes[23], of which at least eleven are classified as putative amino acid transporters[23,24]. Five of these putative amino acid transporters belong to the Apicomplexan amino acid transporter (ApiAT)[25,26] family. This Apicomplexan-specific family of transmembrane transporters can be subdivided into the eleven subfamilies ApiAT1–11. Some of the subfamilies are lineage-specific. For instance, ApiAT4, ApiAT8, ApiAT9 and ApiAT10 are only present in the genomes of *Plasmodium spp*.[1,25]. Others, such as the most ancient variant ApiAT2, can be found in many different Apicomplexan classes[25]. The main feature of the ApiAT family is the possession of multiple, typically twelve, transmembrane domains characteristic of solute transporters with a

signature sequence between transmembrane domains 2 and 3[25]. This classifies them as members of the major facilitator superfamily (MFS)[24,27,28]. However, overall they have limited sequence similarity to other known eukaryotic or prokaryotic transporters[25].

P. falciparum possesses five of the eleven ApiAT subfamilies: *Pf*ApiAT2 (*Pf*ApiAT2/MFR4: PF3D7_0914700), *Pf*ApiAT4 (MFR5: PF3D7_1129900), *Pf*ApiAT8 (NPT1: PF3D7_0104800), *Pf*ApiAT9 (MFR2: PF3D7_0104700) and *Pf*ApiAT10 (MFR3: PF3D7_0312500). Previous work in the rodent malaria species *Plasmodium berghei* (*Pb*) and the related Apicomplexan parasite *Toxoplasma gondii* (*Tg*) showed that *Pb*ApiAT8 (or *Pb*NPT1) and several other *Tg*ApiATs are localized at the PPM[29–32] and possess amino acid transport activity[25,26,29–34]. To date, only *Pb*ApiAT4 has been shown to play an important role in parasite proliferation within erythrocytes[35]. Apart from this, *Pb*ApiAT8 is essential for gametocyte development[29,30,35] and all variants except *Pb*ApiAT2 appear to be necessary for exflagellation of male gametocytes[35]. Additionally, sporozoite development likely requires *Pb*ApiAT2, *Pb*ApiAT4, *Pb*ApiAT9 and *Pb*ApiAT10[35] and a lack of *Pb*ApiAT2 further impairs oocyst development. Furthermore, an association of episomally overexpressed *Pf*ApiAT10-GFP (termed MFR3-GFP) with the mitochondrion has been reported[36].

In this study, we characterize the localization and essentiality of the ApiAT family members of *P. falciparum* during intraerythrocytic development in order to further dissect the function of these unique transporters.

RESULTS

P. falciparum ApiATs localize at the parasite plasma membrane

The five members of the ApiAT family in *P. falciparum* show different gene expression patterns and mRNA levels during the intraerythrocytic developmental cycle (IDC)[37]. While *Pf*ApiAT2 has its maximum transcript level in early ring stage parasites (8 hpi) and *Pf*ApiAT4 and *Pf*ApiAT10 mRNA levels peak in late ring stage parasites (16 hpi), *Pf*ApiAT8 shows a maximum of transcripts in late stage schizonts (48 hpi) and mRNA of *Pf*ApiAT9 is almost absent during the IDC (Figure 1A). Overall, *Pf*ApiAT2 and *Pf*ApiAT4 are most abundantly expressed on mRNA level.

130 To determine their protein expression and localization, we tagged each of the five members
131 of the *Pf*ApiAT family endogenously with GFP using the selection-linked integration (SLI)
132 system[38]. Correct integration of the corresponding targeting plasmids into the respective
133 genomic loci was verified by PCR (Figure S1A). Except for 3D7-ApiAT9-GFP, all generated
134 transgenic cell lines expressed the full-length fusion protein (Figure S1B) to a sufficient level
135 that allowed its subcellular localization. All of them are localized at the PPM (Figure 1B). This
136 localization was confirmed by co-localization with the episomally expressed PPM marker
137 Lyn[39]-mCherry[38] and becomes particularly evident in schizont stage parasites and free
138 merozoites, when PPM and PVM can clearly be separated (Figure 1C).
139 In contrast to published data[36], we also found endogenously GFP-tagged *Pf*ApiAT10 localizing
140 at the PPM. To re-probe into the apparent PPM localization of endogenously GFP-
141 tagged ApiAT10 we also over-expressed this gene as a GFP and mCherry fusion protein
142 using two different promotors (*crt*[40] *or ama1*[41]). This allowed us to assess the influence of the
143 tags as well as differential expression profiles on ApiAT10 protein localization. All cell lines
144 showed PPM localization of the ApiAT10 fusion proteins (Figure 1B-E, S1). Of note,
145 *Pf*ApiAT10-TGD parasites showed also no conferral of drug resistance to Atovaquone (Figure
146 S1B).
147
148 Individual *Pf*ApiATs are not essential for asexual blood stage development
149
150 To probe into the essentiality of the ApiAT family for asexual parasite proliferation, we first
151 targeted the most abundantly expressed *Pf*ApiATs, *Pf*ApiAT2 and *Pf*ApiAT4 by conditional
152 knockdown. Down-regulation was achieved by introducing a glmS ribozyme sequence[40]
153 before the 3'UTR of either the *apiat2* or *apiat4* genomic locus (Figure S1). The ribozyme was
154 activated by addition of 2.5 mM D-(+)-glucosamine hydrochloride (GLCN), which resulted in
155 degradation of mRNA and therefore decreased protein levels. This was assessed and
156 quantified by live cell fluorescence microscopy after two cycles. GLCN treatment resulted in a
157 decreased GFP-fluorescence of 85.9 % ± SD 0.9 for 3D7-*Pf*ApiAT2-GFP or 74.8 % ± SD 14.0 for
158 3D7-*Pf*ApiAT4-GFP (Figure 2A–D) and led to a moderate, but significant reduction of parasite
159 growth of 30–35 % compared to the control (Figure 2E). This data indicates that *Pf*ApiAT2
160 and *Pf*ApiAT4 play a role in efficient blood cell proliferation but imply that they might be non-
161 essential. Therefore, we targeted these genes with deletion constructs using the SLI system[38]

162 that lead to the expression of severely truncated versions of the ApiATs. In this targeted gene
163 disruption (TGD) approach, we also included *Pf*ApiAT8 and *Pf*ApiAT10.
164 Imaging of the TGD cell lines revealed a more diffuse, but still membrane-associated GFP
165 signal (Figure 3A–D). This might be due to the remaining transmembrane domains of the
166 truncated *Pf*ApiAT mutants; however, our approach deleted at least ¾ of their predicted TM
167 domains and thus most likely abolished transporter activity. In concordance with the
168 inducible knockdown data, functional inactivation by truncation of *Pf*ApiAT2 and *Pf*ApiAT4 in
169 the corresponding transgenic cell lines (3D7-ApiAT2-TGD, 3D7-ApiAT4-TGD) led to a
170 moderate decrease of parasite proliferation of 20.2 % ± SD 3.2 and 19.8 % ± SD 8.6 after two
171 parasite replication cycles (Figure 3E). No significant reduction of growth was observed upon
172 disruption of *Pf*ApiAT8 and *Pf*ApiAT10 (Figure 3E). Interestingly, cultivation in amino acid
173 depleted medium (approximately 90 % reduced concentration) did not indicate a higher
174 susceptibility of any of the TGD cell lines to low amino acid concentrations compared to wild
175 type parasites (Figure 3F).
176 To probe into potential transcriptional perturbations within this gene family due to functional
177 inactivation of a single member, quantitative real-time PCR (qPCR) analysis was performed
178 using RNA from four different time points during asexual blood stage replication. However,
179 no consistent upregulation of RNA levels of other *Pf*ApiAT family members was observed in
180 individual *Pf*ApiAT TGDs (Figure S3).
181
182 ***Pf*ApiATs are dispensable during gametocyte development**
183
184 Previous data[30,35] indicated a role of ApiAT8 during gametocyte development of the rodent
185 malaria parasite *P. berghei*. Therefore, we re-engineered the GFP-tagged gene knockdown
186 (Figure S4) and deletion cell lines (Figure S5) for *Pf*ApiAT2, *Pf*ApiAT4, *Pf*ApiAT8 and *Pf*ApiAT10
187 in an inducible gametocyte producing parasite line (3D7-iGP-GDV1GFP-DD[41]) using the same
188 SLI approach. The resulting parasite lines allowed a robust, efficient and synchronized
189 induction of gametocytogenesis and therefore a solid basis for phenotypic analysis. First,
190 using the C-terminal GFP tag, we confirmed expression of all four *Pf*ApiATs in gametocytes.
191 As expected, most *Pf*ApiATs remain PPM localized during gametocytogenesis, which was
192 additionally confirmed by the colocalization with the episomally expressed PPM marker
193 Lyn[39]-mCherry[38] (Figure 4A–F). The exception was *Pf*ApiAT9, which showed only a faint

194 background staining in all gametocyte stages in the 3D7-ApiAT9-GFP line (Figure 4D). The
195 prominent GFP signal at the food vacuole in gametocytes is most likely an unspecific
196 hemozoin signal, as it is also observed in 3D7-iGP control parasites (Figure S4C). Of note,
197 *Pf*ApiAT2 was observed to be strongest expressed in early-stage gametocytes and weaker in
198 late-stages (Figure 5B, D; Figure S4D), while *Pf*ApiAT4 showed strongest expression in late-
199 stage gametocytes (Figure 5C, E). Next, we investigated the consequence of glmS-based
200 conditional knockdown for *Pf*ApiAT2 and *Pf*ApiAT4 (Figure 5A). Although 75–80 % knockdown
201 of *Pf*ApiAT2 or *Pf*ApiAT4 expression was achieved (Figure 5B–E), no significant reduction in
202 gametocytemia or aberrant gametocyte development could be detected (Figure 5F). This was
203 re-investigated by targeted gene disruption. Likewise, deletion of these two genes as well as
204 of *Pf*ApiAT8 and *Pf*ApiAT10 did not result in any measurable impairment of gametocyte
205 development or morphology, indicating the dispensability of these individual *Pf*ApiATs for the
206 sexual stage development of the parasite (Figure 6, Figure S5).
207
208 DISCUSSION
209
210 We localized four putative amino acid transporters (*Pf*ApiAT2, *Pf*ApiAT4 *Pf*ApiAT8, P*f*ApiAT10)
211 of the ApiAT-family to the PPM in asexual blood stage parasites and gametocytes. Due to the
212 low expression of *Pf*ApiAT9-GFP – in agreement with the transcript levels of *apiat9* in these
213 stages[37,42,43] – no conclusive localization could be delivered. The observed PPM localization of
214 the investigated ApiATs is in concordance with published data, since i) the *P. berghei* ApiAT8
215 homologue was shown to be a general cationic amino acid transporter of the PPM[29,30], ii)
216 *Pf*ApiAT8 has recently been localized to the PPM using an overexpression approach[31], and iii)
217 in *T. gondii* several ApiATs (*Tg*ApiAT1, *Tg*ApiAT2, *Tg*ApiAT3-1, *Tg*ApiAT3-2, *Tg*ApiAT3-3,
218 *Tg*ApiAT5-3, *Tg*ApiAT6-1 and *Tg*ApiAT6-3) have been located at the PPM as well[25,29,30,32,33,44].
219 Recent work using episomally overexpressed *Pf*ApiAT10-GFP implied an association of this
220 transporter with the mitochondrial membrane[36] in *Pf*Dd2 parasites. This localization differs
221 from the observed PPM localization of endogenously GFP-tagged *Pf*ApiAT10 in both, 3D7 as
222 well as 3D7-iGP parasites (Figure 1B, 4C, S2A) reported in this study. We confirmed the PPM
223 localization of *Pf*ApiAT10 by its overexpression either as a GFP or mCherry fusion using two
224 different promoters (*crt*[45], *ama1*[46]). In line with that, the reported reduced sensitivity to the
225 mitochondrial electron transport chain inhibitor Atovaquone[47] upon knockout of

226 *Pf*ApiAT10[36], was not observed upon targeted gene disruption in our study (Figure S2B). It is
227 possible but appears unlikely that the reported mitochondrial association as well as reduced
228 sensitivity to atovaquone upon overexpression is due to the different parasite strains
229 (*Pf*Dd2[48] versus 3D7 this study), given that *PfDd2_apiat10* (PFDd2_030017500) has only one
230 silent mutation at position G1080A compared to *Pf3D7_apiat10*[49].
231 During the intraerythrocytic development of the parasite, the amino acid requirements are
232 largely covered by degradation of the globin polypetide[14,50], although – for instance – the
233 import of isoleucine is crucial for the survival of the parasite as *P. falciparum* lacks the
234 canonical pathways for its biosynthesis[51] and adult human hemoglobin lacks this amino acid.
235 Dedicated amino acid transporter could fill this gap. Therefore, we tested the impact of
236 functional inactivation of individual *Pf*ApiATs on parasite growth in asexual and sexual blood
237 stages of *P. falciparum*. We only observed a minor but significant reduction in parasite
238 growth upon knockdown or gene disruption of *Pf*ApiAT2 and *Pf*ApiAT4 in asexual blood
239 stages without compensatory up-regulation of other *Pf*ApiATs on the transcriptional level, as
240 indicated by qPCR analysis. The phenotypes are in agreement with a previously reported
241 reduced parasite multiplication rate of 36 % in *Pb*ApiAT4 knockout parasites[35]. Moreover our
242 data is also in line with the finding that *Pb*ApiAT8 is not essential for asexual
243 replication[29,30,35,52]. This might be explained by functional redundancy either within the ApiAT
244 family, as recently observed for *T. gondii*[34], or by the presence of yet unassigned transporters
245 capable of transporting essential amino acids such as isoleucine across the PPM. Like in *T.*
246 *gondii*, overlapping substrate specificities and lower transport levels might be sufficient for
247 parasite growth *in vitro*[34]. Of note, in *T. gondii* the arginine transporter *Tg*ApiAT1 has been
248 shown to be differently regulated on the translational level in dependence of arginine
249 mediated by an upstream open reading frame (uORF) present on the 5' leader sequence of
250 the transcript[26]. A similar layer of regulation might also be present in *Pf*ApiATs. However,
251 since *Toxoplasma* and *Plasmodium* only share one ApiAT, the likely most ancestral ApiAT2[25],
252 the regulatory elements as well as the general characteristics and substrates of the different
253 *Pf*ApiATs remain largely unknown.
254 Interestingly, a knockout of the ApiAT8 homologue of *P. berghei* (PBANKA_0208300) resulted
255 in strongly reduced number of mature gametocytes with an aberrant morphology of the
256 remaining parasites[30] and strongly reduced exflagellation[35]. In our study, functional
257 inactivation of *Pf*ApiAT8 via targeted gene disruption had no impact on gametocyte

258 development and morphology, which might reflect the pronounced differences in
259 gametocyte development between the rodent infecting *P. berghei* and the human infecting
260 *P. falciparum* parasites[53]. For future work, it will be interesting to target multiple ApiATs by
261 gene disruption in parallel to assess their putative synergy and to probe into *Pf*ApiAT function
262 in other fast-replicating stages of *P. falciparum* such as liver stages, for which the essentiality
263 of several metabolic processes has recently been shown and that primarily rely on the amino
264 acid uptake from their host[54].
265
266 METHODS
267
268 *P. falciparum* culture
269
270 Blood stages of *P. falciparum* 3D7[55] were cultured in human red blood cells (O+ or B+).
271 Cultures were maintained at 37°C in an atmosphere of 1 % O_2, 5 % CO_2 and 94 % N_2 using
272 RPMI complete medium containing 0.5 % Albumax according to standard protocols[56]. In
273 order to obtain highly synchronous parasite cultures late schizonts were isolated by percoll
274 gradient[57] and cultured with fresh erythrocytes for 4 hours. Afterwards sorbitol
275 synchronization[58] was applied in order to remove remaining schizonts resulting in a highly
276 synchronous ring stage parasite culture with a four-hour age window.
277 Induction of gametocytogenesis was done as previously described[41,59]. Briefly, GDV1-GFP-DD
278 expression was achieved by addition of 2 or 4 µM Shield-1 to the culture medium and
279 gametocyte cultures were treated with 50 mM N-acetyl-D-glucosamine (GlcNAc) for five days
280 starting 72 h post Shield-1 addition to eliminate asexual parasites[60]. Alternatively, asexual
281 ring stage cultures with >10 % parasitemia, cultured in the presence of choline, were
282 synchronized with Sorbitol[58] and washed twice in choline-free RPMI medium. Cells were kept
283 in choline-free medium for the entirety of the assay. After one reinvasion cycle cultures at
284 trophozoite stage were treated with 50 mM N-acetyl-D-glucosamine (GlcNAc)[60] and kept on
285 this for five days. Gametocytes were maintained in RPMI complete medium containing 0.25
286 % Albumax and 0.25 % sterile filtered human serum (Interstate Blood Bank, Inc. Memphis,
287 TN, USA).
288 Growth assays in low amino acid medium were performed using amino acid restricted RPMI
289 medium prepared as previously described[20]. Briefly, complete medium was added in a 1/20

290 dilution to amino acid-free RPMI medium 1640 (US Biological, R9010-01). This resulted in a
291 1:20 of the concentration of every amino acid compared to the standard RPMI complete
292 based medium.
293
294 Cloning of plasmid constructs for parasite transfection
295
296 For endogenous tagging using the SLI system[38] and glmS based conditional knockdown[40] a
297 855 (*Pf*ApiAT4/MFR5/PF3D7_1129900) and 1001 bp (*Pf*ApiAT2/MFR4/PF3D7_0914700)
298 homology region was amplified using 3D7 gDNA and cloned into pSLI-PIC1-GFP-glmS[61] using
299 the NotI/MluI restriction site.
300 For endogenous GFP-tagging a 886 bp (*Pf*ApiAT8/NPT1/PF3D7_0104800), 953 bp
301 (*Pf*ApiAT9/MFR2/PF3D7_0104700), 881 bp (*Pf*ApiAT10/MFR3/PF3D7_0312500) homology
302 region was amplified using 3D7 gDNA and cloned into pSLI-GFP[38] using the NotI/MluI
303 restriction site.
304 For SLI-based targeted gene disruption (SLI-TGD) a 396 bp (*Pf*ApiAT4, *Pf*ApiAT8), 402 bp
305 (*Pf*ApiAT9), 393 bp (*Pf*ApiAT10) and 435 bp (*Pf*ApiAT2) homology region was amplified using
306 3D7 gDNA and cloned into the pSLI-TGD plasmid[38] using NotI and MluI restriction sites.
307 For overexpression constructs the full length *Pf*ApiAT10 sequence was amplified from
308 parasite gDNA and cloned into pARL-ama1[46]-AIP-mCherry-yDHODH[61] using the XhoI/KpnI
309 restriction site or into the pARL-crt[45]-PF3D7_0324600-GFP-hDHFR[37] plasmid using the
310 KpnI/AvrII restriction site. Oligonucleotides used to generate the DNA fragments are
311 summarized in Table S1.
312 For co-localization experiments the plasmid pLyn-FRB-mCherry[38] was used.
313
314 Western blot analysis
315
316 Immunoblots were performed using saponin-lysed, infected erythrocytes. Parasite proteins
317 were separated on a 12 % SDS-PAGE gel as described previously[62,63] and transferred to a
318 nitrocellulose membrane (Amersham Protran; 0.45-µm pore nitrocellulose membrane; GE
319 Healthcare) using a Trans-Blot device (Bio-Rad) according to the manufacturer's instructions.
320 The membranes were blocked with 3 % skim milk in TBS for 30 minutes and then probed with
321 mouse anti-GFP (clone 7.1 and 13.1; 1:1,000, Roche) or rabbit anti-aldolase[64] (1:2,000). The

322 chemiluminescent signal of the horseradish peroxidase-coupled secondary antibodies
323 (Dianova) was visualized using a Chemi Doc XRS imaging system (Bio-Rad) and processed with
324 Image Lab 5.2 software (Bio-Rad).
325 To perform loading controls and ensure equal loading of parasite material, rabbit anti-
326 aldolase[64] antibodies were used. The corresponding immunoblots were incubated twice in
327 stripping buffer (0.2 M glycine, 50 mM dithiothreitol, 0.05 % Tween 20) at 55°C for 1 h and
328 washed 3 times with Tris-buffered saline for 10 min before re-probing.
329
330 Transfection of *P. falciparum*
331
332 For transfection, Percoll-purified[57] parasites at late schizont stage were transfected with 50
333 µg plasmid DNA using Amaxa Nucleofector 2b (Lonza, Switzerland) as previously described[65].
334 Transfectants were selected using either 4 nM WR99210 (Jacobus Pharmaceuticals), 0.9 µM
335 DSM1[66] (BEI Resources), or 2 µg/mL blasticidin S (Life Technologies, USA). In order to select
336 for parasites carrying the genomic modification via the SLI system[38], G418 (ThermoFisher,
337 USA) at a final concentration of 400 µg/mL was added to a culture with about 5 %
338 parasitemia. The selection process and integration test were performed as previously
339 described[38].
340
341 Imaging
342
343 All fluorescence images were captured using a Zeiss Axioskop 2plus microscope with a
344 Hamamatsu Digital camera (Model C4742-95) or a Leica D6B fluorescence microscope
345 equipped with a Leica DFC9000 GT camera and a Leica Plan Apochromat 100x/1.4 oil
346 objective.
347 Microscopy of live parasite-infected erythrocytes was performed as previously described[67].
348 Briefly, parasites were incubated in standard culture medium with 1 µg/mL Hoechst-33342
349 (Invitrogen) for 15 minutes at 37°C prior to imaging. 5.4 µL of infected erythrocytes were
350 added on a glass slide and covered with a cover slip. Nuclei were stained with 1 µg/mL
351 Hoechst-33342 (Invitrogen). Mitochondria were visualized by incubation of parasites with 20
352 nM MitoTracker Red 665 CMXRos (Invitrogen) for 15 min at 37°C prior to imaging. Images

353 were processed using Fiji[68] and Adobe Photoshop CC 2021 was used for display purposes
354 only.
355
356 Growth assay
357
358 For growth assays of TGD cell lines a flow cytometry assay, adapted from previously
359 published assays[69,70], was performed to measure proliferation over five days. For growth
360 under low amino acid conditions TGD and wild type cell lines were cultured in parallel in
361 standard and amino acid-depleted medium for five days. Each day parasite cultures were
362 resuspended and 20 µL samples were transferred to an Eppendorf tube. 80 µL RPMI
363 containing Hoechst-33342 and dihydroethidium (DHE) was added to obtain final
364 concentrations of 5 µg/mL and 4.5 µg/mL, respectively. Samples were incubated for 20 min
365 (protected from UV light) at room temperature, and parasitemia was determined using an
366 LSRII flow cytometer by counting 100,000 events using the FACSDiva software (BD
367 Biosciences) or using an ACEA NovoCyte flow cytometer.
368
369 Gametocyte quantification assay
370
371 Giemsa-stained blood smears at day 10 post induction of GDV1 expression were obtained
372 and at least 10 fields of view were recorded using a 63x objective per treatment and time
373 point. Erythrocyte numbers were then determined using the automated Parasitemia
374 software (http://www.gburri.org/parasitemia/) while the number of gametocytes was
375 determined manually in >700 erythrocytes per sample.
376
377 GlmS-based knockdown
378
379 GlmS-based knockdown assay was adapted from previously published assays[40,71]. To induce
380 knockdown, highly synchronous early ring stage parasites were split in two dishes, 2.5 mM
381 glucosamine was added to one of them and parasite growth was measured by FACS after two
382 and four parasite replication cycles. Parasite cultures were inspected daily by Giemsa smears
383 and, if necessary, diluted to avoid growth bias caused by high parasitemia. As an additional
384 control, the same amount of glucosamine was also added to 3D7 wildtype parasites. For all

385 analyses, medium was changed daily, and fresh glucosamine was added every day. GlmS-
386 based knockdown assay was adapted from previously published assays[40,71]. To induce
387 knockdown, highly synchronous early ring stage parasites were split into two dishes, 2.5 mM
388 glucosamine was added to one of them and parasite growth was measured by FACS after two
389 and four parasite replication cycles. Parasite cultures were inspected daily by Giemsa smears
390 and, if necessary, diluted to avoid growth bias caused by high parasitemia. As an additional
391 control, the same amount of glucosamine was also added to 3D7 wildtype parasites. For all
392 analyses, medium was changed daily, and fresh glucosamine was added every day.
393 Knockdown was quantified by fluorescence live cell microscopy using schizonts about 40 h
394 post glucosamine treatment. Parasites with similar size were imaged, and fluorescence was
395 captured with the same acquisition settings to obtain comparable measurements of the
396 fluorescence intensity. Fluorescence intensity (integrated density) was measured with Fiji[68],
397 and background was subtracted in each image. The data was visualized with GraphPad Prism
398 version 8 (GraphPad Software, USA).
399 For knockdown experiments in gametocytes synchronized ring stage cultures were induced
400 by the addition of Shield-1, as described above. At day 3 post induction the culture was spilt
401 into two dishes and one dish was cultured in the presence of 2.5 mM glucosamine for the
402 remaining ten days. Knockdown was quantified by fluorescence live cell microscopy at day 7
403 and 10 post induction, as described above.
404
405 Drug assays
406
407 Drug assays were adapted from previously described assays[72–74]. Briefly, 3D7-iGP and 3D7-
408 iGP-ApiAT10-TGD parasites were synchronized to a 4 h time window resulting in 0–4 h ring
409 stage parasites. At 24 hpi, parasitemia was determined by flow cytometry and the drug
410 susceptibility assays were set up in black 96-well microtiter plates (Thermo Scientific) with 0.1
411 % starting parasitemia and 2 % hematocrit in a final volume of 200 µl. In each plate, infected
412 erythrocytes in the absence of drugs treated with DMSO only served as positive controls,
413 while uninfected RBCs served as negative controls (for background subtraction). Parasites
414 were incubated with varying concentrations of dihydroartemisinin (DHA) (Adipogen,
415 Switzerland, AG-CN2-0468) (0–50 nM) and Atovaquone (Cayman, Item No.23802) (0–16 nM).

416 After 96 h of incubation, parasite growth was determined by measuring the fluorescence of
417 SYBR Gold (Invitrogen). Therefore, 100 µl/well supernatant was discarded without disturbing
418 the RBC layer and 100 µl of lysis buffer (20 mM Tris, 0.008 % saponin, 0.08 % Triton X-100, 1x
419 SYBR Gold) was added to each well. Plates were incubated in the dark for 2 h at room
420 temperature before measuring fluorescence using the EnVision Multimode Plate Reader
421 (PerkinElmer), as described previously[74]. In order to calculate IC_{50} values, the measured
422 values were normalized to the uninfected erythrocytes and plotted in GraphPad Prism
423 version 8 (GraphPad Software, USA) as % of DMSO control. Dose-response curves were
424 generated using nonlinear regression (curve fit > dose-response inhibition > (log) inhibitor vs.
425 normalized response—variable slope).
426
427 Quantitative real-time PCR (qPCR)
428
429 Parasites at different time-points (8, 16, 32 and 44 hpi) were harvested for 3D7-ApiAT2-TGD,
430 3D7-ApiAT4-TGD, 3D7-ApiAT8-TGD, 3D7-ApiAT10-TGD and 3D7-WT to obtain RNA samples
431 for quantitative real-time PCR. Highly synchronous ring stage parasite cultures were grown
432 for another 40 h and TRIzol samples were harvested in the following cycle. Volumes of
433 prewarmed TRIzol used for infected erythrocyte lysis and storage of RNA samples depended
434 on the parasite stage: ring stages were lysed in 5x volumes, trophozoites in 10x volumes and
435 schizonts in 20x volumes of the settled cell pellet. RNA was purified and checked for absence
436 of genomic DNA. cDNA synthesis with random hexamers and quantitative real-time PCR was
437 performed exactly as previously described[75]. Primers for each of the *apiat* genes, for genes to
438 control for parasite stages (*sbp1*[76]*, tom22*, *ama1*) and for housekeeping genes (*arginyl-tRNA*
439 *synthetase*[75], *fructose bisphosphate aldolase*[77]) are listed in Table S1. Amplification
440 efficiencies of the primer pairs were determined over six log10 dilutions of gDNA (10 ng –
441 0.0001 ng) and were shown to have similar values between 1.915 and 2.001 (Table S1).
442 Expression of *apiat* genes and controls were analyzed in relation to expression of the *arginyl-*
443 *tRNA synthetase* gene (normalizer).
444
445 Software
446

447 Schematic protein representations were designed using IBS[78], predicted protein domains
448 were obtained from plasmodDB[79] inferred from TMHMM[80]. Parasite icons were generated
449 using BioRender (biorender.com). Statistical analyses were performed with GraphPad Prism
450 version 8 (GraphPad Software, USA).
451
452 **Acknowledgements**
453
454 We thank Till Voss for 3D7-iGP parasites, Jacobus Pharmaceuticals for WR99210 and Greg
455 Burri for the parasitemia software. DSM1 (MRA-1161) was obtained from MR4/BEI
456 Resources, NIAID, NIH.
457
458 **Author contribution**
459
460 Conceptualization: JSW, JS, TWG, AB; Methodology: JSW, EP, PCB, PMR, TS, JS, TWG, AB;
461 Investigation: JSW, CVG, GF, JMR, EP, JLF, HVT, SS, PCB; Formal Analysis: JS, AB; Writing
462 original manuscript: JSW, AB; Review & Editing: JSW, TWG, AB; Funding Acquisition: TWG, AB,
463 JS; Resources: PMR, TS; Project Administration: TWG, AB; Supervision: TWG, AB. All authors
464 read and approved the manuscript.
465
466 **Funding**
467
468 AB and JSW were funded by the German Research Foundation (DFG) grant BA 5213/3-1. This
469 project was also supported by Partnership of Universität Hamburg and DESY (PIER) project ID
470 PIF-2018-87 and by a Joachim Herz Foundation Project grant. JLF is supported by a HFSPO
471 long-term postdoctoral fellowship (LT000024/2020-L). PCB was funded by the Deutsche
472 Forschungsgemeinschaft (DFG, German Research Foundation) – project number 414222880.
473
474 **Figures**
475
476 **Figure 1: *P. falciparum* ApiATs localize to the parasite plasma membrane (PPM) during asexual**
477 **blood stage development. (A)** Heatmap of RNA-seq gene expression profiles[37] of *Pf*ApiAT2,
478 *Pf*ApiAT4, *Pf*ApiAT8, *Pf*ApiAT9 and *Pf*ApiAT10 during the asexual blood stage development.

479 Timepoints indicated as hours post infection (hpi) plus merozoites (m). **(B)** Localization of
480 *Pf*ApiAT2-GFP, *Pf*ApiAT4-GFP, *Pf*ApiAT8-GFP, *Pf*ApiAT9-GFP and *Pf*ApiAT10-GFP by live-cell
481 microscopy across the IDC of 3D7 parasites. **(C)** Co-localization of the GFP-tagged ApiAT
482 fusion proteins with the PPM marker protein lyn-mCherry in schizonts and merozoites. **(D)**
483 Live-cell microscopy of 3D7-crt-ApiAT10-GFP parasites across the IDC. **(E)** 3D7-iGP-ApiAT10-
484 GFP/ama1-ApiAT10-mCherry parasites at trophozoite and schizont stage. Nuclei were stained
485 with Hoechst-33342. Scale bar, 2 µm. Parasite stages as indicated; ring stage (R), early
486 trophozoite (ET), late trophozoite (LT) and schizont (S).
487
488 **Figure 2: Conditional knockdown of *Pf*ApiAT2 and *Pf*ApiAT4 reveals a minor growth defect**
489 **during asexual blood stage development. (A, B)** Live-cell microscopy of **(A)** 3D7-ApiAT2-GFP
490 and **(B)** 3D7-ApiAT4-GFP parasites, which were treated for 40 hours with 2.5 mM
491 glucosamine (GLCN) or that were left untreated (control). Scale bar, 2 µm. **(C, D)**
492 Quantification of knockdown efficiency by measuring mean fluorescence intensity (MFI)
493 density and parasite size (area) of **(C)** 3D7-ApiAT2-GFP and **(D)** 3D7-ApiAT4-GFP parasites 40
494 hours after treatment with or without 2.5 mM glucosamine. Data is displayed as mean +/- SD
495 of three independent experiments and individual data points are displayed on a scatterplot
496 color-coded by experiments according to Superplot guidelines[81]. P-values displayed were
497 determined using a two-tailed unpaired t-test with Welch's correction. **(E)** Growth of
498 parasites treated with or without 2.5 mM GLCN after two and four parasite replication cycles
499 as determined by flow cytometry. Shown are relative parasitemia values, which were
500 obtained by dividing the parasitemia of glucosamine-treated cultures by the parasitemia of
501 the corresponding untreated ones. Displayed are means +/- SD of independent growth
502 experiments with the number of experiments (n) indicated. Adjusted p-values displayed were
503 determined with a two-tailed unpaired t-test with Welch's correction and using the
504 Benjamini-Hochberg correction afterwards accounting for multiple testing by comparing
505 ApiAT2-GFP-glmS or ApiAT4-GFP-glmS cultured with 2.5mM GLCN to 3D7 parasites cultured
506 with 2.5mM GLCN.
507
508 **Figure 3: Targeted gene disruption (TGD) of *Pf*ApiAT2, *Pf*ApiAT4, *Pf*ApiAT8 and *Pf*ApiAT10**
509 **reveals the dispensability of *Pf*ApiATs for *in vitro* parasite proliferation. (A–D)** Schematic
510 representation of the full-length and truncated protein versions (upper panel). Protein length

511 (number of amino acids) and putative transmembrane protein domains (blue) are indicated.
512 Localization of **(A)** *Pf*ApiAT8-TGD-GFP, **(B)** *Pf*ApiAT4-TGD-GFP, **(C)** *Pf*ApiAT2-TGD-GFP and **(D)**
513 *Pf*ApiAT10-TGD in ring, trophozoite and schizont stage parasites is shown in lower panels.
514 Nuclei were stained with Hoechst-33342. Scale bar, 2 µm. **(E)** Growth of 3D7-ApiAT-TGD cell
515 lines as percentage of 3D7 parasites growth, monitored over two intracellular development
516 cycles by flow cytometry. The number of independent growth experiments (n) per 3D7-
517 ApiAT-TGD cell line is indicated. 3D7 wildtype parasites were measured in parallel. Statistical
518 differences were analyzed using a one-sample t-test with Benjamini-Hochberg correction
519 accounting for multiple comparisons. **(F)** Growth of TGD and 3D7 cell lines cultivated in low
520 amino acid medium relative to their growth in standard medium is shown as percentage of
521 growth after two parasite replication cycles. The number of individual growth experiments
522 (n) performed is indicated for each 3D7-ApiAT-TGD line, additionally 3D7 wildtype parasites
523 were analyzed with n=9. No statistical differences were observed by comparing relative
524 growth of TGD cell lines to 3D7 using a two-tailed unpaired t-test with Bonferroni correction.
525
526 **Figure 4: *P. falciparum* ApiATs localize to the parasite plasma membrane (PPM) during**
527 **gametocyte development. (A–D)** Localization of **(A)** *Pf*ApiAT2-GFP, **(B)** *Pf*ApiAT4-GFP, **(C)**
528 *Pf*ApiAT8-GFP and **(D)** *Pf*ApiAT10-GFP in individual 3D7-iGP-ApiAT-GFP cell lines during
529 gametocyte development (stage I - V) as determined by live-cell microscopy. White arrow
530 heads indicate remaining GDV1-GFP signal observed in close proximity to the Hoechst signal
531 in the 3D7-iGP-ApiAT8-GFP cell line **(C)**, as previously described[59,82,83]. **(E)** Localization of
532 *Pf*ApiAT9-GFP during gametocytogenesis was assessed with the 3D7-ApiAT9-GFP cell line (see
533 Figure 1) upon induction with choline depletion. **(F)** Co-localization of the GFP-tagged ApiAT
534 fusion proteins with the PPM marker protein lyn-mCherry. Nuclei were stained with Hoechst-
535 33342. Scale bar, 2 µm.
536
537 **Figure 5: Conditional knockdown of *Pf*ApiAT2 and *Pf*ApiAT4 reveals dispensability for**
538 **gametocyte development. (A)** Schematic representation of the experimental setup. **(B, C)**
539 Live-cell microscopy of parasites with identical settings of **(B)** 3D7-iGP-ApiAT2-GFP and **(C)**
540 3D7-iGP-ApiAT4-GFP stage I – V gametocytes. Scale bar, 2 µm. **(D, E)** Quantification of
541 knockdown by measuring mean fluorescence intensity (MFI) density and size (area) of **(D)**
542 3D7-iGP-ApiAT2-GFP **(E)** 3D7-iGP-ApiAT4-GFP parasites at day 7 and day 12 post induction of

543 gametocytogenesis cultured either with or without (control) 2.5 mM GLCN. Scale bar, 2 µm.
544 Data are displayed as mean +/- SD of three (3D7-iGP-ApiAT2-GFP) or four (3D7-iGP-ApiAT4-
545 GFP) independent experiments and individual data points are displayed on a scatterplot
546 color-coded by experiments according to Superplots guidelines[81]. P-values displayed were
547 determined with a two-tailed unpaired t-test with Welch's correction. **(F)** For each condition
548 gametocytemia at day 10 post gametocyte induction was determined by counting between
549 702-7693 (mean 2210) cells per condition in Giemsa-stained thin blood smears. The relative
550 gametocytemia values (%) displayed were obtained by dividing the gametocytemia of
551 glucosamine-treated cultures by the gametocytemia of the corresponding untreated
552 cultures. Displayed are means +/- SD of independent growth experiments with the number of
553 experiments (n) indicated. A two-tailed unpaired t-test with Welch's and Benjamini-Hochberg
554 correction was used to calculate multiplicity adjusted p-values for ApiAT2-GFP-glmS or
555 ApiAT4-GFP-glmS versus 3D7-iGP parasites all cultured with 2.5mM GLCN.
556
557 **Figure 6: Targeted gene disruption (TGD) of *Pf*ApiAT2, *Pf*ApiAT4, *Pf*ApiAT8 and *Pf*ApiAT10**
558 **reveals dispensability of ApiATs for gametocyte development.** Representative images from two
559 (*Pf*ApiAT2, *Pf*ApiAT4) or three (*Pf*ApiAT8, *Pf*ApiAT10) independent experiments derived from
560 Giemsa-stained thin blood smears of gametocyte stages I-V of 3D7-iGP, 3D7-iGP-ApiAT2-TGD,
561 3D7-iGP-ApiAT4-TGD, 3D7-iGP-ApiAT8-TGD, 3D7-iGP-ApiAT10-TGD parasites. Scale bar, 5 µm.
562
563 **Figure S1: PCR analysis and western blots of 3D7-ApiAT-GFP and 3D7-ApiAT-TGD cell lines. (A)**
564 PCR-based analysis of unmodified wildtype (WT) and transgenic knock-in (KI) cell lines (3D7-
565 ApiAT2-GFP-glmS, 3D7-ApiAT4-GFP-glmS, 3D7-ApiAT8-GFP, 3D7-ApiAT9-GFP, 3D7-ApiAT10-
566 GFP). Specific genomic modifications resulting from correct integration of the respective SLI-
567 based vectors were tested targeting the 3'- and 5'-end of the locus. **(B)** Western blot analysis
568 of wildtype (3D7) and knock-in (KI) cell lines (3D7-ApiAT2-GFP-glmS, 3D7-ApiAT4-GFP-glmS,
569 3D7-ApiAT8-GFP, 3D7-ApiAT10-GFP) using mouse anti-GFP to detect the tagged full-length
570 protein (upper panel) and rabbit anti-aldolase to control for equal loading (lower panel).
571 Protein sizes are indicated in kDa. **(C)** PCR-based analysis of unmodified wildtype (WT) and
572 transgenic parasites modified by targeted gene disruption (TGD).
573

574 **Figure S2: *Pf*ApiAT10 is PPM localized and its functional inactivation has no influence on**
575 Atovaquone sensitivity. (A) Live-cell microscopy of 3D7-iGP-ApiAT10-GFP parasites stained
576 with MitoTracker Red CMXRos across the IDC and in gametocytes. Stages as indicated: R =
577 ring stage, ET = early trophozoite, LT = late trophozoite, ES = early schizont, LS = late schizont,
578 G = gametocyte; Nuclei were stained with Hoechst-33342. Scale bar, 2 µm. **(B)** Drug
579 susceptibility assays of 3D7-iGP and 3D7-iGP-ApiAT10-TGD parasites were performed with
580 Atovaquone (left) and dihydroartemisinin (DHA, right). Parasite growth was determined by
581 measuring the DNA content using SYBR gold when exposed to varying concentrations of
582 drugs for 96 h. The growth of DMSO-treated control parasites was set to 100%. Shown are
583 means +/- SD of 4 or 5 independent biological replicates performed in technical duplicates.
584 Calculated IC_{50} values with 95% confidence intervals are shown above each graph.
585
586 **Figure S3: Quantitative real-time PCR of individual *Pf*ApiAT-encoding genes and controls in**
587 **3D7-ApiAT-TGD and wildtype parasites.** Expression of *apiat* genes and control genes (*sbp1*,
588 *tom22*, *ama1*, *fructose-bisphosphate aldolase*) normalized to the housekeeping control
589 *arginyl-tRNA synthetase* over four different time points during intraerythrocytic development
590 cycle of *P. falciparum* parasites. Bars with individual measurements from n=2 (3D7-ApiAT2-
591 TGD, 3D7-ApiAT4-TGD) or n=3 (3D7-ApiAT8, 3D7-ApiAT10, 3D7 wildtype) biological
592 replicates. Gene accession numbers, primer sequences and amplification efficiencies are
593 listed in Table S1.
594
595 **Figure S4: PCR analysis of 3D7-iGP-ApiAT-GFP cell lines and Giemsa smears from *Pf*ApiAT2 and**
596 ***Pf*ApiAT4 conditional knockdown experiments. (A)** PCR-based analysis of unmodified wildtype
597 (WT) and transgenic knock-in (KI) cell lines (3D7-iGP-ApiAT2-GFP-glmS, 3D7-iGP-ApiAT4-GFP-
598 glmS, 3D7-iGP-ApiAT8-GFP, 3D7-iGP-ApiAT10-GFP). **(B)** Giemsa smears of stage I – V 3D7-iGP-
599 ApiAT2-GFP-glmS and 3D7-iGP-ApiAT4-GFP-glmS gametocytes cultured either without
600 (control) or with 2.5 mM glucosamine (GLCN). Scale bar, 5 µm. **(C)** Live cell imaging of 3D7-
601 iGP stage IV and V gametocytes. Nuclei were stained with Hoechst-33342. Scale bar, 2 µm.
602 **(D)** Live cell microscopy of 3D7-iGP-ApiAT2 stage IV and V gametocytes from Figure 5B, with
603 adjusted brightness. Scale bar, 2 µm.
604

605 **Figure S5: PCR analysis of 3D7-iGP-ApiAT-TGD cell lines and Giemsa smears from 3D7-iGP-**
606 **ApiAT8-TGD stage IV and V gametocytes showing normal morphology. (A)** PCR-based analysis
607 of unmodified wildtype (WT) and transgenic TGD cell lines (3D7-iGP-ApiAT2-TGD, 3D7-iGP-
608 ApiAT4-TGD, 3D7-iGP-ApiAT8-TGD, 3D7-iGP-ApiAT10-TGD). (**B**) Giemsa smears of 3D7-iGP-
609 ApiAT8-TGD and 3D7-iGP stage IV and V gametocytes from three independent experiments.
610 Scale bar, 5 µm.
611
612 **Table S1: Oligonucleotides used for cloning and quantitative real-time PCR (qPCR).**
613
614 **References**

615 1. Krishnan, A. & Soldati-Favre, D. Amino acid metabolism in apicomplexan parasites.
616 *Metabolites* **11**, 1–17 (2021).
617 2. Wrenger, C. *et al.* Specific inhibition of the aspartate aminotransferase of plasmodium
618 falciparum. *J. Mol. Biol.* **405**, 956–971 (2011).
619 3. Nagaraj, V. A. *et al.* Asparagine requirement in Plasmodium berghei as a target to
620 prevent malaria transmission and liver infections. *Nat. Commun.* **6**, 1–13 (2015).
621 4. Meireles, P. *et al.* Uptake and metabolism of arginine impact Plasmodium
622 development in the liver. *Sci. Rep.* **7**, (2017).
623 5. MacRae, J. I. *et al.* Mitochondrial metabolism of glucose and glutamine is required for
624 intracellular growth of toxoplasma gondii. *Cell Host Microbe* **12**, 682–692 (2012).
625 6. Sopitthummakhun, K. *et al.* Plasmodium serine hydroxymethyltransferase as a
626 potential anti-malarial target: Inhibition studies using improved methods for enzyme
627 production and assay. *Malar. J.* **11**, 194 (2012).
628 7. Spielmann, T., Gras, S., Sabitzki, R. & Meissner, M. Endocytosis in Plasmodium and
629 Toxoplasma Parasites. *Trends in Parasitology* **36**, 520–532 (2020).
630 8. Kirk, K. & Lehane, A. M. Membrane transport in the malaria parasite and its host
631 erythrocyte. *Biochem. J.* **457**, 1–18 (2014).
632 9. Divo, A. A., Geary, T. G., Davis, N. L. & Jensen, J. B. Nutritional Requirements of
633 Plasmodium falciparum in Culture. I. Exogenously Supplied Dialyzable Components
634 Necessary for Continuous Growth. *J. Protozool.* **32**, 59–64 (1985).
635 10. Ginsburg, H., Kutner, S., Krugliak, M. & Ioav Cabantchik, Z. Characterization of
636 permeation pathways appearing in the host membrane of Plasmodium falciparum

637 infected red blood cells. *Mol. Biochem. Parasitol.* **14**, 313–322 (1985).
638 11. Kirk, K., Horner, H. A., Elford, B. C., Ellory, J. C. & Newbold, C. I. Transport of diverse
639 substrates into malaria-infected erythrocytes via a pathway showing functional
640 characteristics of a chloride channel. *J. Biol. Chem.* **269**, 3339–3347 (1994).
641 12. Olszewski, K. L. *et al.* Host-Parasite Interactions Revealed by Plasmodium falciparum
642 Metabolomics. *Cell Host Microbe* **5**, 191–199 (2009).
643 13. Liu, J., Istvan, E. S., Gluzman, I. Y., Gross, J. & Goldberg, D. E. Plasmodium falciparum
644 ensures its amino acid supply with multiple acquisition pathways and redundant
645 proteolytic enzyme systems. *Proc. Natl. Acad. Sci. U. S. A.* **103**, 8840–8845 (2006).
646 14. Babbitt, S. E. *et al.* Plasmodium falciparum responds to amino acid starvation by
647 entering into a hibernatory state. *Proc. Natl. Acad. Sci. U. S. A.* **109**, E3278–E3287
648 (2012).
649 15. McLean, K. J. & Jacobs-Lorena, M. The response of Plasmodium falciparum to
650 isoleucine withdrawal is dependent on the stage of progression through the
651 intraerythrocytic cell cycle. *Malar. J.* **19**, 147 (2020).
652 16. Martin, R. E. & Kirk, K. Transport of the essential nutrient isoleucine in human
653 erythrocytes infected with the malaria parasite Plasmodium falciparum. *Blood* **109**,
654 2217–2224 (2007).
655 17. Cobbold, S. A., Martin, R. E. & Kirk, K. Methionine transport in the malaria parasite
656 Plasmodium falciparum. *Int. J. Parasitol.* **41**, 125–135 (2011).
657 18. Desai, S. A., Krogstad, D. J. & McCleskey, E. W. A nutrient-permeable channel on the
658 intraerythrocytic malaria parasite. *Nature* **362**, 643–646 (1993).
659 19. Desai, S. A. & Rosenberg, R. L. Pore size of the malaria parasite's nutrient channel.
660 *Proc. Natl. Acad. Sci. U. S. A.* **94**, 2045–2049 (1997).
661 20. Mesén-Ramírez, P. *et al.* EXP1 is critical for nutrient uptake across the parasitophorous
662 vacuole membrane of malaria parasites. *PLoS Biol.* **17**, e3000473 (2019).
663 21. Garten, M. *et al.* EXP2 is a nutrient-permeable channel in the vacuolar membrane of
664 Plasmodium and is essential for protein export via PTEX. *Nat. Microbiol.* 1 (2018).
665 doi:10.1038/s41564-018-0222-7
666 22. Counihan, N. A., Modak, J. K. & de Koning-Ward, T. F. How Malaria Parasites Acquire
667 Nutrients From Their Host. *Front. Cell Dev. Biol.* **9**, 582 (2021).
668 23. Martin, R. E. The transportome of the malaria parasite. *Biol. Rev. Camb. Philos. Soc.* **95**,

669 305–332 (2020).
670 24. Martin, R. E., Henry, R. I., Abbey, J. L., Clements, J. D. & Kirk, K. The 'permeome' of the
671 malaria parasite: an overview of the membrane transport proteins of Plasmodium
672 falciparum. *Genome Biol.* **6**, R26 (2005).
673 25. Parker, K. E. R. *et al.* The tyrosine transporter of Toxoplasma gondii is a member of the
674 newly defined apicomplexan amino acid transporter (ApiAT) family. *PLoS Pathog.* **15**,
675 e1007577 (2019).
676 26. Rajendran, E. *et al.* Substrate-mediated regulation of the arginine transporter of
677 Toxoplasma gondii. *PLoS Pathog.* **17**, e1009816 (2021).
678 27. Reddy, V. S., Shlykov, M. A., Castillo, R., Sun, E. I. & Saier, M. H. The major facilitator
679 superfamily (MFS) revisited. *FEBS J.* **279**, 2022–2035 (2012).
680 28. Pao, S. S., Paulsen, I. T. & Saier, M. H. Major Facilitator Superfamily. *Microbiol. Mol.*
681 *Biol. Rev.* **62**, 1–34 (1998).
682 29. Rajendran, E. *et al.* Cationic amino acid transporters play key roles in the survival and
683 transmission of apicomplexan parasites. *Nat. Commun.* **8**, 1–13 (2017).
684 30. Boisson, B. *et al.* The novel putative transporter NPT1 plays a critical role in early
685 stages of Plasmodium berghei sexual development. *Mol. Microbiol.* **81**, 1343–1357
686 (2011).
687 31. Blomqvist, K. *et al.* Influence of Plasmodium falciparum Calcium-Dependent Protein
688 Kinase 5 (PfCDPK5) on the Late Schizont Stage Phosphoproteome. *mSphere* **5**, (2020).
689 32. Kloehn, J., Lunghi, M., Varesio, E., Dubois, D. & Soldati-Favre, D. Untargeted
690 Metabolomics Uncovers the Essential Lysine Transporter in Toxoplasma gondii.
691 *Metabolites* **11**, 476 (2021).
692 33. Wallbank, B. A. *et al.* Characterisation of the *Toxoplasma gondii* tyrosine transporter
693 and its phosphorylation by the calcium-dependent protein kinase 3. *Mol. Microbiol.*
694 **111**, 1167–1181 (2019).
695 34. Fairweather, S. J. *et al.* Coordinated Action of Multiple Transporters in the Acquisition
696 of Essential Cationic Amino Acids by the Intracellular Parasite Toxoplasma gondii 2 3
697 Running Title: Essential Cationic Amino Acid Transporters in Toxoplasma parasites.
698 *bioRxiv* 2021.06.25.450001 (2021). doi:10.1101/2021.06.25.450001
699 35. Kenthirapalan, S., Waters, A. P., Matuschewski, K. & Kooij, T. W. A. Functional profiles
700 of orphan membrane transporters in the life cycle of the malaria parasite. *Nat.*

701 *Commun.* **7**, 10519 (2016).
702 36. Rocamora, F. *et al.* PfMFR3: A Multidrug-Resistant Modulator in Plasmodium
703 falciparum. *ACS Infect. Dis.* acsinfecdis.0c00676 (2021).
704 doi:10.1021/acsinfecdis.0c00676
705 37. Wichers, J. S. *et al.* Dissecting the gene expression, localization, membrane topology,
706 and function of the plasmodium falciparum STEVOR protein family. *MBio* **10**, e01500-
707 19 (2019).
708 38. Birnbaum, J. *et al.* A genetic system to study Plasmodium falciparum protein function.
709 *Nat. Methods* **14**, 450–456 (2017).
710 39. Inoue, T., Heo, W. Do, Grimley, J. S., Wandless, T. J. & Meyer, T. An inducible
711 translocation strategy to rapidly activate and inhibit small GTPase signaling pathways.
712 *Nat. Methods* **2**, 415–418 (2005).
713 40. Prommana, P. *et al.* Inducible Knockdown of Plasmodium Gene Expression Using the
714 glmS Ribozyme. *PLoS One* **8**, e73783 (2013).
715 41. Boltryk, S. D. *et al.* CRISPR/Cas9-engineered inducible gametocyte producer lines as a
716 valuable tool for Plasmodium falciparum malaria transmission research. *Nat. Commun.*
717 **12**, 4806 (2021).
718 42. Otto, T. D. *et al.* New insights into the blood-stage transcriptome of Plasmodium
719 falciparum using RNA-Seq. *Mol. Microbiol.* **76**, 12–24 (2010).
720 43. López-Barragán, M. J. *et al.* Directional gene expression and antisense transcripts in
721 sexual and asexual stages of Plasmodium falciparum. *BMC Genomics* **12**, 587 (2011).
722 44. Sangaré, L. O. *et al.* Unconventional endosome-like compartment and retromer
723 complex in Toxoplasma gondii govern parasite integrity and host infection. *Nat.*
724 *Commun.* **7**, 1–14 (2016).
725 45. Struck, N. S. *et al.* Re-defining the Golgi complex in Plasmodium falciparum using the
726 novel Golgi marker PfGRASP. *J. Cell Sci.* **118**, 5603–5613 (2005).
727 46. Hu, G. *et al.* Transcriptional profiling of growth perturbations of the human malaria
728 parasite Plasmodium falciparum. *Nat. Biotechnol.* **28**, 91–98 (2010).
729 47. Fry, M. *et al.* Novel anti-malarial hydroxynaphthoquinones with potent broad
730 spectrum anti-protozoal activity. *Parasitology* **90**, 45–55 (1985).
731 48. Wellems, T., Oduola, A. M., Fenton, B., Desjardins, R. & Panton, L. Chromosome size
732 variation occurs in cloned Plasmodium falciparum on in vitro cultivation. *Rev. bras.*

733 *genét* **11**, 813–25 (1988).
734 49. Otto, T. D. *et al.* Long read assemblies of geographically dispersed Plasmodium
735 falciparum isolates reveal highly structured subtelomeres. *Wellcome open Res.* **3**, 52
736 (2018).
737 50. Goldberg, D. E. Complex nature of malaria parasite hemoglobin degradation.
738 *Proceedings of the National Academy of Sciences of the United States of America* **110**,
739 5283–5284 (2013).
740 51. Payne, S. H. & Loomis, W. F. Retention and loss of amino acid biosynthetic pathways
741 based on analysis of whole-genome sequences. *Eukaryot. Cell* **5**, 272–276 (2006).
742 52. Sayers, C. P., Mollard, V., Buchanan, H. D., McFadden, G. I. & Goodman, C. D. A genetic
743 screen in rodent malaria parasites identifies five new apicoplast putative membrane
744 transporters, one of which is essential in human malaria parasites. *Cell. Microbiol.* **20**,
745 e12789 (2018).
746 53. Ngotho, P. *et al.* Revisiting gametocyte biology in malaria parasites. *FEMS Microbiol.*
747 *Rev.* **43**, 401–414 (2019).
748 54. Stanway, R. R. *et al.* Genome-Scale Identification of Essential Metabolic Processes for
749 Targeting the Plasmodium Liver Stage. *Cell* **179**, 1112-1128.e26 (2019).
750 55. Walliker, D. *et al.* Genetic analysis of the human malaria parasite Plasmodium
751 falciparum. *Science (80-.).* **236**, 1661–6 (1987).
752 56. Trager, W. & Jensen, J. B. Continuous culture of Plasmodium falciparum: its impact on
753 malaria research. *Int. J. Parasitol.* **27**, 989–1006 (1997).
754 57. Rivadeneira, E., Wasserman, M. & Espinal, C. Separation and Concentration of
755 Schizonts of Plasmodium falciparum by Percoll Gradients. *J. Protozool.* **30**, 367–370
756 (1983).
757 58. Lambros, C. & Vanderberg, J. P. Synchronization of Plasmodium falciparum
758 Erythrocytic Stages in Culture. *J. Parasitol.* **65**, 418 (1979).
759 59. Filarsky, M. *et al.* GDV1 induces sexual commitment of malaria parasites by
760 antagonizing HP1-dependent gene silencing. *Science (80-.).* **359**, 1259–1263 (2018).
761 60. Ponnudurai, T., Lensen, A. H. W., Meis, J. F. G. M. & Meuwissen, J. H. E.
762 Synchronization of Plasmodium falciparum gametocytes using an automated
763 suspension culture system. *Parasitology* **93**, 263–274 (1986).
764 61. Wichers, J. S. *et al.* Identification of novel inner membrane complex and apical annuli

765 proteins of the malaria parasite Plasmodium falciparum. *Cell. Microbiol.* **23**, e13341
766 (2021).
767 62. Bachmann, A. *et al.* A comparative study of the localization and membrane topology of
768 members of the RIFIN, STEVOR and PfMC-2TM protein families in Plasmodium
769 falciparum-infected erythrocytes. *Malar. J.* **14**, 274 (2015).
770 63. Heiber, A. & Spielmann, T. Preparation of Parasite Protein Extracts and Western Blot
771 Analysis. *BIO-PROTOCOL* **4**, (2014).
772 64. Mesén-Ramírez, P. *et al.* Stable Translocation Intermediates Jam Global Protein Export
773 in Plasmodium falciparum Parasites and Link the PTEX Component EXP2 with
774 Translocation Activity. *PLoS Pathog.* **12**, e1005618 (2016).
775 65. Moon, R. W. *et al.* Adaptation of the genetically tractable malaria pathogen
776 Plasmodium knowlesi to continuous culture in human erythrocytes. *Proc. Natl. Acad.*
777 *Sci.* **110**, 531–536 (2013).
778 66. Ganesan, S. M. *et al.* Yeast dihydroorotate dehydrogenase as a new selectable marker
779 for Plasmodium falciparum transfection. *Mol. Biochem. Parasitol.* **177**, 29–34 (2011).
780 67. Grüring, C. & Spielmann, T. Imaging of live malaria blood stage parasites. *Methods*
781 *Enzymol.* **506**, 81–92 (2012).
782 68. Schindelin, J. *et al.* Fiji: an open-source platform for biological-image analysis. *Nat.*
783 *Methods* **9**, 676–682 (2012).
784 69. Malleret, B. *et al.* A rapid and robust tri-color flow cytometry assay for monitoring
785 malaria parasite development. *Sci. Rep.* **1**, 118 (2011).
786 70. Jonscher, E. *et al.* PfVPS45 Is Required for Host Cell Cytosol Uptake by Malaria Blood
787 Stage Parasites. *Cell Host Microbe* **25**, 166-173.e5 (2019).
788 71. Burda, P.-C. *et al.* Structure-Based Identification and Functional Characterization of a
789 Lipocalin in the Malaria Parasite Plasmodium falciparum. *Cell Rep.* **31**, 107817 (2020).
790 72. Burda, P.-C. *et al.* Global analysis of putative phospholipases in the malaria parasite
791 Plasmodium 1 falciparum reveals critical factors for parasite proliferation 2 3. *bioRxiv*
792 2021.06.28.450158 (2021). doi:10.1101/2021.06.28.450158
793 73. Smilkstein, M., Sriwilaijaroen, N., Kelly, J. X., Wilairat, P. & Riscoe, M. Simple and
794 Inexpensive Fluorescence-Based Technique for High-Throughput Antimalarial Drug
795 Screening. *Antimicrob. Agents Chemother.* **48**, 1803–1806 (2004).
796 74. Schwed, S. I., Alder, A., Gilberger, T. & Kunick, C. 4-Arylthieno[2,3-b]pyridine-2-

797 carboxamides Are a New Class of Antiplasmodial Agents. *Molecules* **25**, (2020).
798 75. Bachmann, A. *et al.* Controlled human malaria infection with Plasmodium falciparum
799 demonstrates impact of naturally acquired immunity on virulence gene expression.
800 *PLOS Pathog.* **15**, e1007906 (2019).
801 76. Petter, M. *et al.* Expression of P. falciparum var genes involves exchange of the histone
802 variant H2A.Z at the promoter. *PLoS Pathog.* **7**, (2011).
803 77. Salanti, A. *et al.* Selective upregulation of a single distinctly structured var gene in
804 chondroitin sulphate A-adhering Plasmodium falciparum involved in pregnancy-
805 associated malaria. *Mol. Microbiol.* **49**, 179–191 (2003).
806 78. Liu, W. *et al.* IBS: An illustrator for the presentation and visualization of biological
807 sequences. *Bioinformatics* **31**, 3359–3361 (2015).
808 79. Aurrecoechea, C. *et al.* PlasmoDB: a functional genomic database for malaria parasites.
809 *Nucleic Acids Res.* **37**, D539–D543 (2009).
810 80. Sonnhammer, E. L., von Heijne, G. & Krogh, A. A hidden Markov model for predicting
811 transmembrane helices in protein sequences. *Proceedings. Int. Conf. Intell. Syst. Mol.*
812 *Biol.* **6**, 175–82 (1998).
813 81. Lord, S. J., Velle, K. B., Mullins, R. D. & Fritz-Laylin, L. K. SuperPlots: Communicating
814 reproducibility and variability in cell biology. *J. Cell Biol.* **219**, (2020).
815 82. Tibúrcio, M. *et al.* A 39-Amino-Acid C-Terminal Truncation of GDV1 Disrupts Sexual
816 Commitment in Plasmodium falciparum. *mSphere* **6**, (2021).
817 83. Eksi, S. *et al.* Plasmodium falciparum Gametocyte Development 1 (Pfgdv1) and
818 Gametocytogenesis Early Gene Identification and Commitment to Sexual
819 Development. *PLoS Pathog.* **8**, (2012).
820

Figure 1

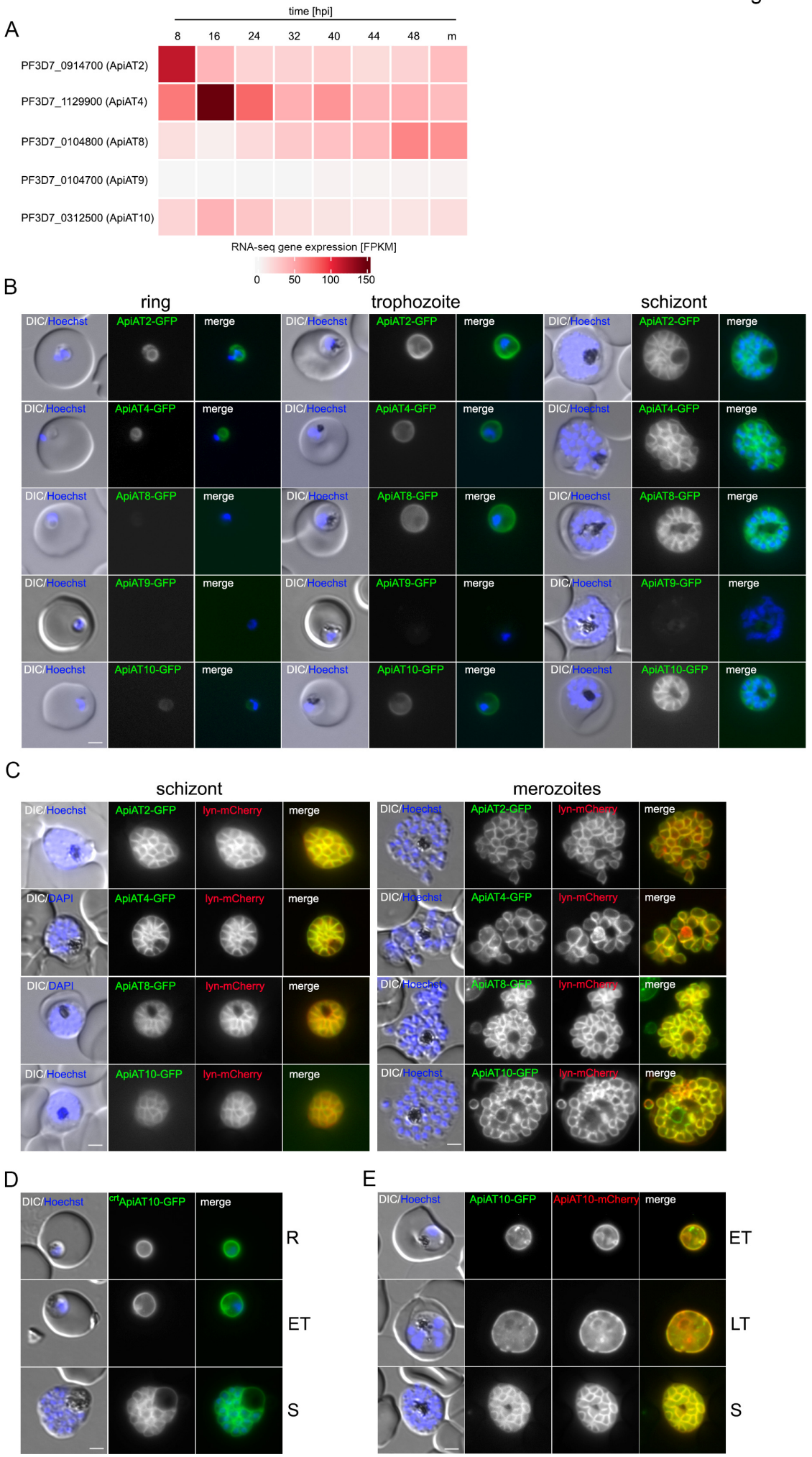
A
time [hpi]
8
16
24
32
40
44
48
m
PF3D7_0914700 (ApiAT2)
PF3D7_1129900 (ApiAT4)
PF3D7_0104800 (ApiAT8)
PF3D7_0104700 (ApiAT9)
PF3D7_0312500 (ApiAT10)
RNA-seq gene expression [FPKM]
0
50
100
150
B
ring
trophozoite
schizont
DIC/Hoechst
ApiAT2-GFP
merge
ApiAT4-GFP
ApiAT8-GFP
ApiAT9-GFP
ApiAT10-GFP
C
schizont
merozoites
DIC/DAPI
lyn-mCherry
D
cytApiAT10-GFP
R
ET
S
E
ApiAT10-mCherry
LT

Figure 2

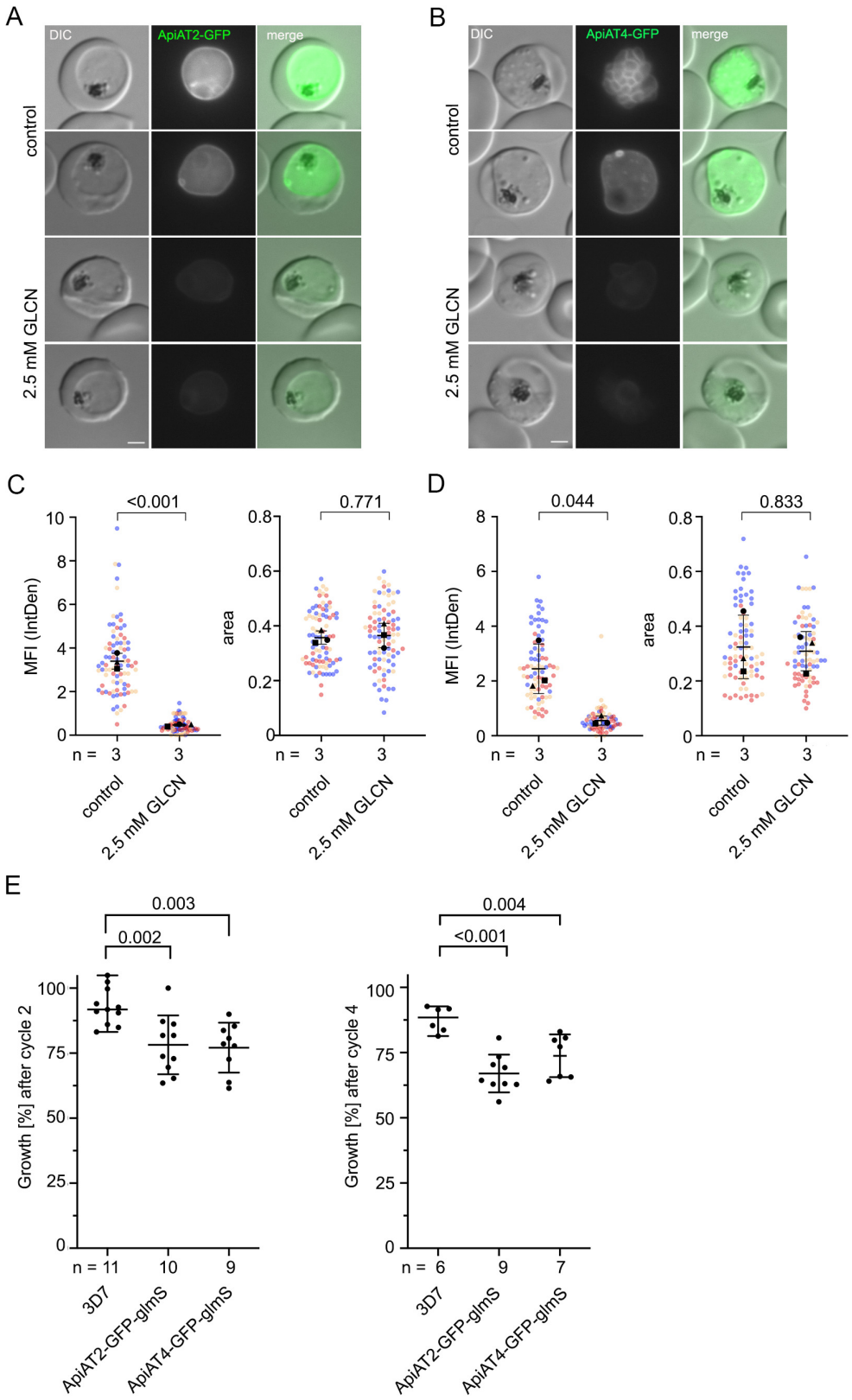
A
DIC
ApiAT2-GFP
merge
control
2.5 mM GLCN
B
DIC
ApiAT4-GFP
merge
control
2.5 mM GLCN
C
<0.001
0.771
MFI (IntDen)
area
n = 3 3
control
2.5 mM GLCN
D
0.044
0.833
MFI (IntDen)
area
n = 3 3
control
2.5 mM GLCN
E
0.003
0.002
Growth [%] after cycle 2
n = 11 10 9
3D7
ApiAT2-GFP-glmS
ApiAT4-GFP-glmS
0.004
<0.001
Growth [%] after cycle 4
n = 6 9 7
3D7
ApiAT2-GFP-glmS
ApiAT4-GFP-glmS

Figure 3

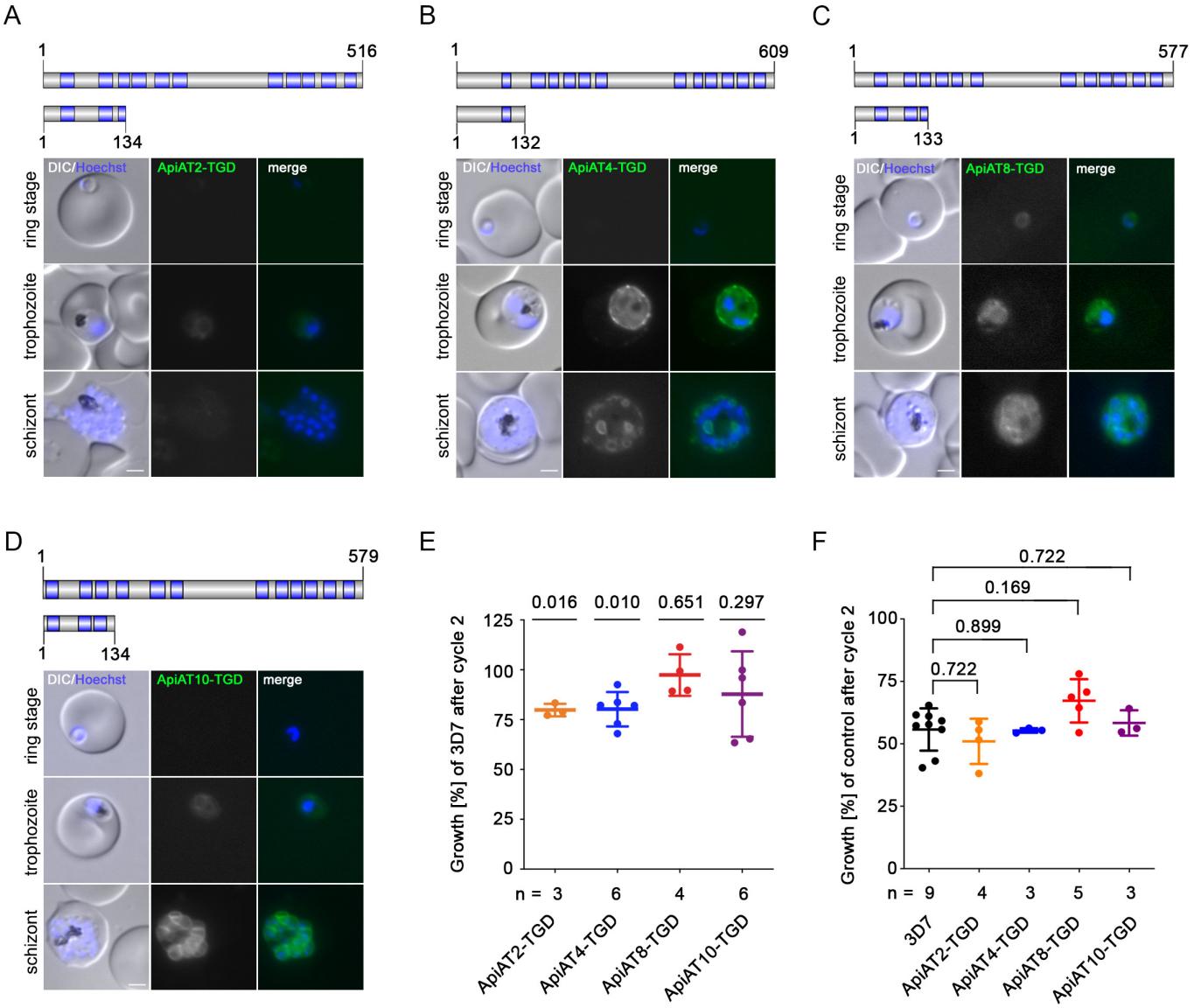
A
1
516
1
134
DIC/Hoechst
ApiAT2-TGD
merge
ring stage
trophozoite
schizont
B
1
609
1
132
DIC/Hoechst
ApiAT4-TGD
merge
ring stage
trophozoite
schizont
C
1
577
1
133
DIC/Hoechst
ApiAT8-TGD
merge
ring stage
trophozoite
schizont
D
1
579
1
134
DIC/Hoechst
ApiAT10-TGD
merge
ring stage
trophozoite
schizont
E
Growth [%] of 3D7 after cycle 2
0.016
0.010
0.651
0.297
125
100
75
50
25
0
n = 3
6
4
6
ApiAT2-TGD
ApiAT4-TGD
ApiAT8-TGD
ApiAT10-TGD
F
Growth [%] of control after cycle 2
0.722
0.169
0.899
0.722
100
75
50
25
0
n = 9
4
3
5
3
3D7
ApiAT2-TGD
ApiAT4-TGD
ApiAT8-TGD
ApiAT10-TGD

Figure 4

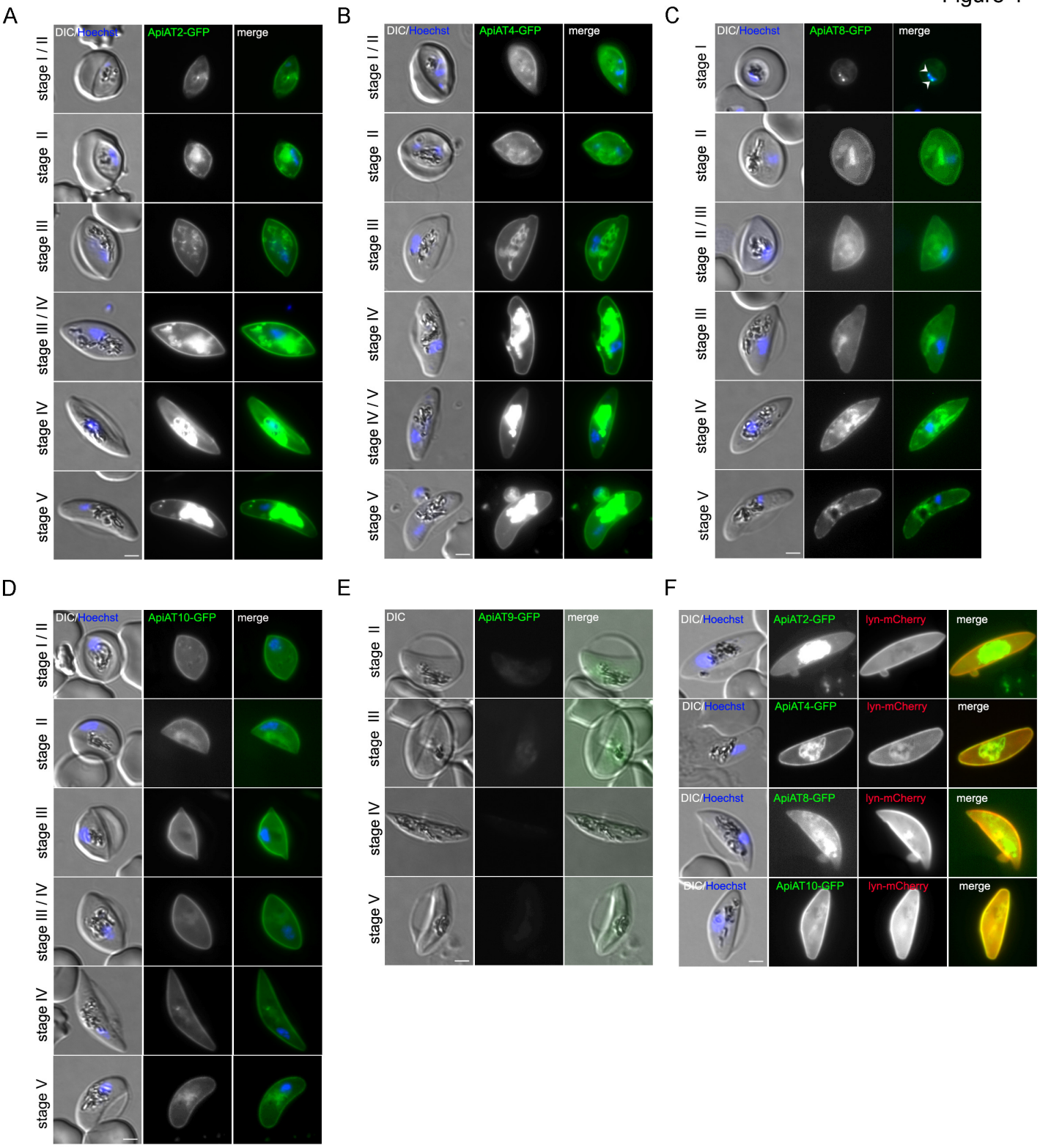
A
DIC/Hoechst
ApiAT2-GFP
merge
stage I / II
stage II
stage III
stage III / IV
stage IV
stage V
B
DIC/Hoechst
ApiAT4-GFP
merge
stage I / II
stage II
stage III
stage IV
stage IV / V
stage V
C
DIC/Hoechst
ApiAT8-GFP
merge
stage I
stage II
stage II / III
stage III
stage IV
stage V
D
DIC/Hoechst
ApiAT10-GFP
merge
stage I / II
stage II
stage III
stage III / IV
stage IV
stage V
E
DIC
ApiAT9-GFP
merge
stage II
stage III
stage IV
stage V
F
DIC/Hoechst
ApiAT2-GFP
lyn-mCherry
merge
DIC/Hoechst
ApiAT4-GFP
lyn-mCherry
merge
DIC/Hoechst
ApiAT8-GFP
lyn-mCherry
merge
DIC/Hoechst
ApiAT10-GFP
lyn-mCherry
merge

Figure 5

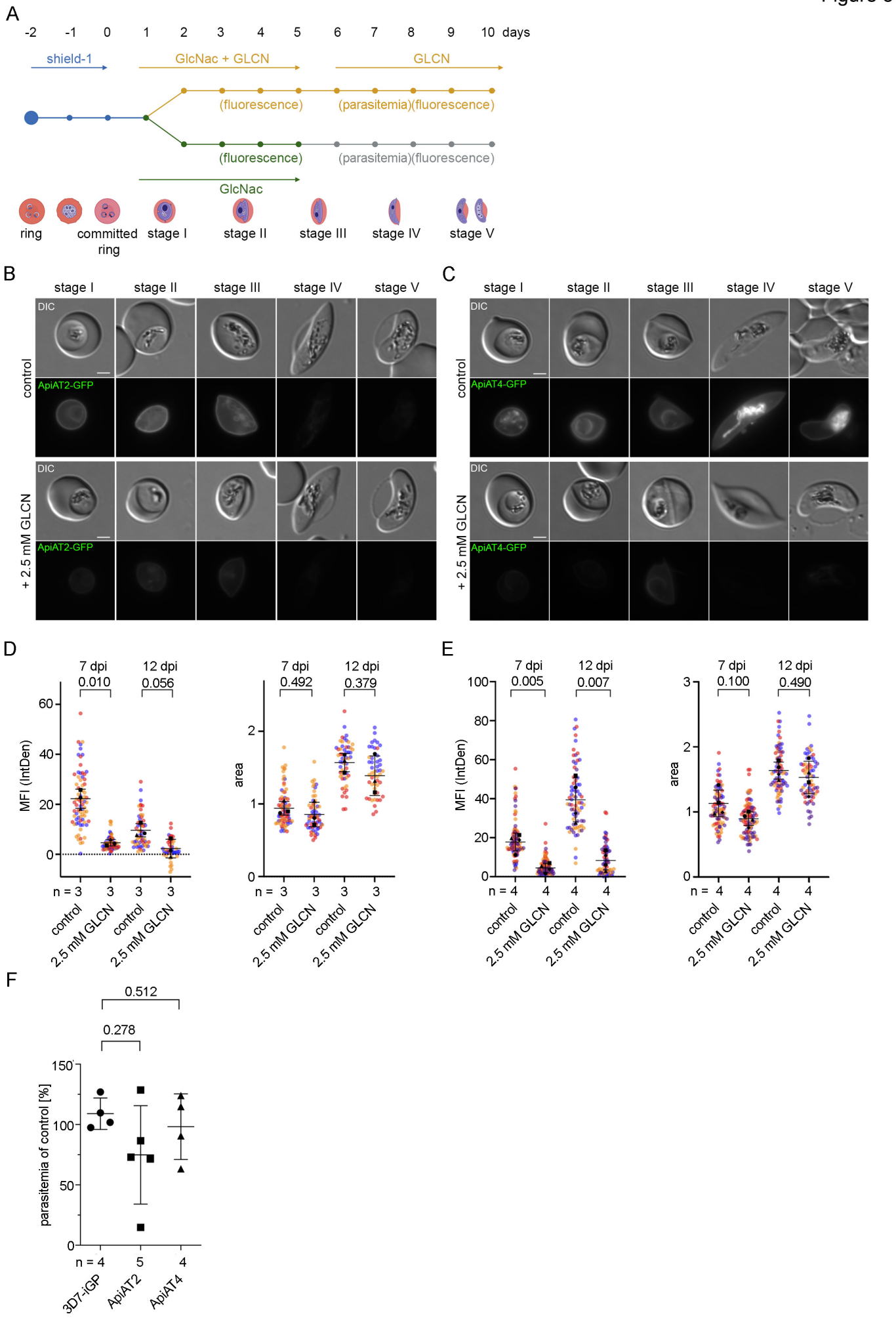
A
-2 -1 0 1 2 3 4 5 6 7 8 9 10 days
shield-1
GlcNac + GLCN
GLCN
(fluorescence)
(parasitemia)(fluorescence)
(fluorescence)
(parasitemia)(fluorescence)
GlcNac
ring
committed ring
stage I
stage II
stage III
stage IV
stage V
B
stage I
stage II
stage III
stage IV
stage V
DIC
control
ApiAT2-GFP
+ 2.5 mM GLCN
C
ApiAT4-GFP
D
7 dpi
12 dpi
0.010
0.056
MFI (IntDen)
0.492
0.379
area
n = 3
control
2.5 mM GLCN
E
0.005
0.007
0.100
0.490
n = 4
F
0.512
0.278
parasitemia of control [%]
3D7-iGP
ApiAT2
ApiAT4

Figure 6

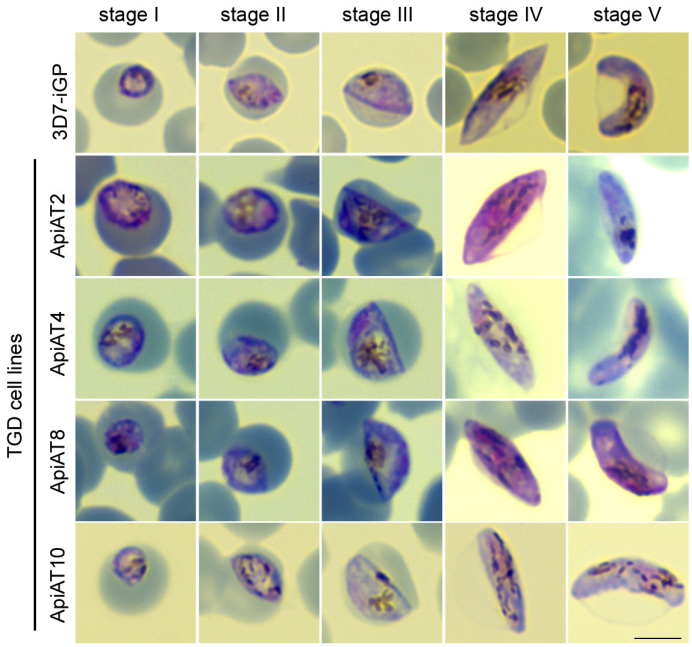
stage I
stage II
stage III
stage IV
stage V
3D7-iGP
ApiAT2
ApiAT4
ApiAT8
ApiAT10
TGD cell lines